Biosensors and Bioelectronics 86 (2016) 369–376

Contents lists available at ScienceDirect

Biosensors and Bioelectronics

journal homepage: www.elsevier.com/locate/bios

A Nanostructured Bifunctional platform for Sensing of Glucose Biomarker in Artificial Saliva: Synergy in hybrid Pt/Au surfaces

Paulo A. Raymundo-Pereira [a,*], Flávio M. Shimizu [b], Dyovani Coelho [a], Maria H.O. Piazzeta [c], Angelo L. Gobbi [c], Sergio A.S. Machado [a], Osvaldo N. Oliveira Jr. [b]

[a] São Carlos Institute of Chemistry, University of São Paulo, CP 380, CEP 13566–590, São Carlos, São Paulo, Brazil
[b] São Carlos Institute of Physics, University of São Paulo, CP 369, CEP 13560–970, São Carlos, São Paulo, Brazil
[c] Laboratório de Microfabricação, Laboratório Nacional de Nanotecnologia, Centro Nacional de Pesquisa em Energia e Materiais/CNPEM, Campinas, SP, Brazil

ARTICLE INFO

Article history:
Received 3 May 2016
Received in revised form
10 June 2016
Accepted 18 June 2016
Available online 23 June 2016

Keywords:
Hybrid Surface
Bimetallic
Nanostructured platform
Biosensing
Bifunctional Surface

ABSTRACT

We report on a bimetallic, bifunctional electrode where a platinum (Pt) surface was patterned with nanostructured gold (Au) fingers with different film thicknesses, which was functionalized with glucose oxidase (GOx) to yield a highly sensitive glucose biosensor. This was achieved by using selective adsorption of a self-assembled monolayer (SAM) onto Au fingers, which allowed GOx immobilization only onto the Au-SAM surface. This modified electrode was termed bifunctional because it allowed to simultaneously immobilize the biomolecule (GOx) on gold to catalyze glucose, and detect hydrogen peroxide on Pt sites. Optimized electrocatalytic activity was reached for the architecture Pt/Au-SAM/GOx with 50 nm thickness of Au, where synergy between Pt and Au allowed for detection of hydrogen peroxide (H_2O_2) at a low applied potential (0 V vs. Ag/AgCl). Detection was performed for H_2O_2 in the range between 4.7 and 102.7 nmol L^{-1}, with detection limit of 3.4×10^{-9} mol L^{-1} (3.4 nmol L^{-1}) and an apparent Michaelis-Menten rate constant of 3.2×10^{-6} mol L^{-1}, which is considerably smaller than similar devices with monometallic electrodes. The methodology was validated by measuring glucose in artificial saliva, including in the presence of interferents. The synergy between Pt and Au was confirmed in electrochemical impedance spectroscopy measurements with an increased electron transfer, compared to bare Pt and Au electrodes. The approach for fabricating the reproducible bimetallic Pt/Au electrodes is entirely generic and may be explored for other types of biosensors and biodevices where advantage can be taken of the combination of the two metals.

1. INTRODUCTION

One important goal in nanochemistry is to develop synthetic pathways to tailor physicochemical properties of nanomaterials (Yoo and Park, 2007), such as bimetallic nanostructures that may possess enhanced catalytic(Carrette et al., 2000; Park et al., 2003), electronic(Trindade et al., 2001), mechanical(Link et al., 1999), optical(Freeman et al., 1996; Sanedrin et al., 2005) and magnetic (Aliev et al., 1999; Cho et al., 2004) characteristics, in comparison to their monometallic counterparts(Jia et al., 2015; Karthikeyan and Murugavelu, 2012; Rashid et al., 2015; Wojtysiak et al., 2014). Bimetallic nanostructures are promising as electrocatalysts, dehydrogenation catalysts and selective oxidants(Jia et al., 2015), in addition to serving as platforms for label-free biodevices (Yang et al., 2014; Yu et al., 2013). Gold (Au) and platinum (Pt) are the most used in bimetallic structures for (bio)sensors(Pumera et al., 2007; Wang, 2005) since gold is capable of forming a self-assembled monolayer with an alkanethiol via the gold-sulfur bond (Au-S) to create a biocompatible environment(Du et al., 2007; Kang et al., 2007; Manso et al., 2008; Mott et al., 2007; Qian and Yang, 2006; Wu et al., 2007), while platinum is suitable for electrocatalysis of oxidation/reduction of H_2O_2(Evans et al., 2002; Ferapontova et al., 2001; Hrapovic et al., 2004; Wu et al., 2006; Yang et al., 2006). Nanostructured Pt/Au surfaces are expected to yield electrochemical sensors that are highly selective, sensitive and with fast response time. Indeed, top-down and bottom-up strategies were used to obtain modified Pt/Au electrodes and detect a nuclear matrix protein 22 (NMP22) with a limit of detection of 3.33 pg/mL(Jia et al., 2015). Electrodeposited Au/Pt nanoparticles onto 3-aminopropyltriethoxy silane were exploited to determine H_2O_2 produced by acetylcholinesterase/choline oxidase (Upadhyay et al., 2009).

* Corresponding author.
E-mail address: pauloaugustoraymundopereira@gmail.com (P.A. Raymundo-Pereira).

http://dx.doi.org/10.1016/j.bios.2016.06.053
0956-5663/

The nanostructures in the examples above, however, are fabricated with time-consuming, many-step procedures, besides displaying low reproducibility and repeatability. Other requirements to fabricate suitable electrodes for detecting H_2O_2, which is a target analyte since it is generated by reactions catalyzed by oxidoreductase enzymes in the presence of oxygen(Kung et al., 2014), include to lower the potential and avoid interference from other electroactive species. For a high overpotential ($\sim +0.7$ V vs. Ag/AgCl) is needed to generate the oxidation current of H_2O_2 for neat Pt, and interferents in human blood such as ascorbic acid and uric acid are electroactive at this potential(Chen et al., 2012b; Kung et al., 2014). Redox mediators have been used to solve these problems, thus yielding efficient electrochemical enzyme biosensors (Ricci and Palleschi, 2005).

In this study, we build upon previous knowledge on redox mediators and electrochemical sensors with bimetallic nanostructures to produce a glucose biosensor with immobilized glucose oxidase (GOx), in which the main novelty lies in the fine control of the Pt catalytic activity by patterning its surface with interdigitated gold fingers. We show that synergy in biosensing is achieved with a suitable architecture where GOx was immobilized selectively on Au, and H_2O_2 was detected on the Pt surface.

2. EXPERIMENTAL PROCEDURES

2.1. Materials

All the reagents were of analytical grade and used without further purification. Sulfuric acid of high purity (96%) was obtained from Merck. Potassium chloride (KCl), glucose, *N*-(3-Dimethylaminopropyl)-*N'*-ethylcarbodiimide hydrochloride (EDC), *N*-Hydroxysuccinimide (NHS) and 11-mercaptoundecanoic acid (MUA) were purchased from Sigma-Aldrich. Anydrous potassium ferricyanide and trihydrate potassium ferrocyanide were obtained from J. T. Baker and Mallinckrodt. High-purity deionised water (resistivity of 18.2 MΩcm) was obtained from a Milli-Q system (Millipore). The experiments were performed at room temperature of approximately 25 °C. The enzyme glucose oxidase (GOx) from *Aspergillus niger* (3.0 mg mL^{-1}) was purchased from Sigma-Aldrich. Phosphate buffer solution (PBS) at pH 7.0 was prepared with Na_2HPO_4 and NaH_2PO_4 (Sigma-Aldrich). The initial amount of GOx contained in the vessel was diluted with PBS, aliquoted into Eppendorf® microtubes and frozen until use. The glucose solution (1.0 mmol L^{-1}) was prepared in 0.1 mol L^{-1} PBS solution and stored at 0.1 mol L^{-1}.

2.2. Characterization Techniques

The structure and morphology of the bimetallic Pt/Au nanostructured surface was examined by scanning electron microscopy coupled to an energy-dispersive X-ray spectroscopy (SEM-EDX) operating at 20.0 kV, with images recorded with a LEO-440 microscope (Zeiss-Leica). The samples were fixed to solid supports with a conducting double-faced carbon tape and coated with a 20 nm thick carbon layer. These surfaces were also analyzed with atomic force microscopy (AFM) using a Nanosurf EasyScan 2 AFM System (Nanosurf AG), where the topographic images were obtained with the non-contact/tapping mode for a fixed area of 55 μm^2, a long cantilever with a force constant of 48 N m^{-1} and resonance frequency of 190 kHz (model Tap190Al-G).

Electrochemical measurements were performed using a model PGSTAT 302 Autolab electrochemical system (Eco Chimie) and controlled by GPES 4.9.7 software. All measurements were carried out in a 25 mL thermostated glass cell at 25 °C, with a three-electrode configuration: the bimetallic Pt/Au surface as the working electrode (geometric area 0.283 cm^2), a Ag/AgCl (3 mol L^{-1} KCl) as a reference and a platinum foil (1.0 cm^2) as an auxiliary electrode. The solution within the cell was neither stirred nor aerated during the measurements. Electrochemical impedance spectroscopy (EIS) data were acquired with a PGSTAT 302 system, controlled by FRA2 software, in the frequency range between 0.1 Hz and 100 kHz with amplitude of 10 mV and under open circuit potential (OCP) conditions in 0.1 mol L^{-1} KCl solution containing 5.0 mmol L^{-1} of $K_3[Fe(CN)_6]/K_4[Fe(CN)_6]$(Wojtysiak et al., 2014).

2.3. Pretreatment of the gold and platinum electrodes

The bare Au and Pt electrodes were submitted to a 2-step pretreatment procedure(Coelho and Machado, 2014) adapted from Tkac and Davis(Tkac and Davis, 2008): (i) the electrode was immersed in a "piranha" solution (1:3 v/v H_2O_2: H_2SO_4) during 300 s and then (ii) submitted to several cycles in a potential range between 0.0 and 1.7 V for Au and between −0.23 and 1.30 V for Pt electrodes, in 0.5 mol L^{-1} H_2SO_4 solution(Coelho and Machado, 2014; Tkac and Davis, 2008).

2.4. Patterning Pt with nanostructured Au films

A 5 nm adhesive layer of chromium was deposited on glass slides, followed by a 100 nm layer of platinum. The patterning of Pt substrates with Au nanostructured films was performed with photolithographic and lift-off processes. The first step consisted in depositing a layer of positive photoresist AZ4210 on BK7 glass slides coated with Pt (on top of the chromium adhesive layer) using a spin coater with the rotation speed of 3000 rpm for 30 s, followed by heat treatment at 90 °C for 300 s and exposed to an interdigitated pattern with UV light for 40 s. Then, the substrate was immersed in a developing solution (K400) for 15 s. The pattern in the photoresist film was coated with an Au layer, whose thickness could be 20, 50 and 100 nm. The excess photoresist and Au were removed using the lift-off procedure which consists in immersing the substrate in acetone, thus yielding an Au-patterned Pt surface referred to here as Pt/Au bimetallic electrode. Fig. 1 (A) shows the experimental set-up.

2.5. Self-assembled monolayers (SAM) of the alkanethiol

A SAM of alkanethiol was obtained by immersing the Pt/Au bimetallic electrode in an ethanol solution containing 5.0×10^{-3} mol L^{-1} of MUA for 20 h, following the procedures established in ref.(Coelho and Machado, 2014). Then, the electrode was washed with ethanol to remove unbound thiols, rinsed with Milli-Q water and dried at room temperature. The Pt/Au bimetallic electrodes coated with a MUA-SAM are referred to as Pt/Au/SAM. The geometric area (0.283 cm^2) of the Pt/Au/SAM surface was defined using a galvanoplastic adhesive tape Type 470 (3 M) according to the methodology developed by Hideko's group(Cavalcanti et al., 2012; Uliana et al., 2011). The electrical contact was made under platinum on the opposite side as shown in Fig. 1 (B).

2.6. Electrochemical performance of the Pt/Au/SAM electrode

The bimetallic (Pt/Au) surface coated with a MUA-SAM was submitted to 100 cyclic scans at 1.0 V s^{-1} in 0.5 mol L^{-1} H_2SO_4 solution between −0.23 and X (where X = 0.9, 1.0, 1.1 and 1.2) V. This procedure was performed to remove the SAM from the Pt area (i.e. with the SAM remaining only onto Au area). With SAM deposited only on Au, the biomolecules (glucose oxidase) will be restricted to these regions, as indicated in Fig. 2. Consequently, no

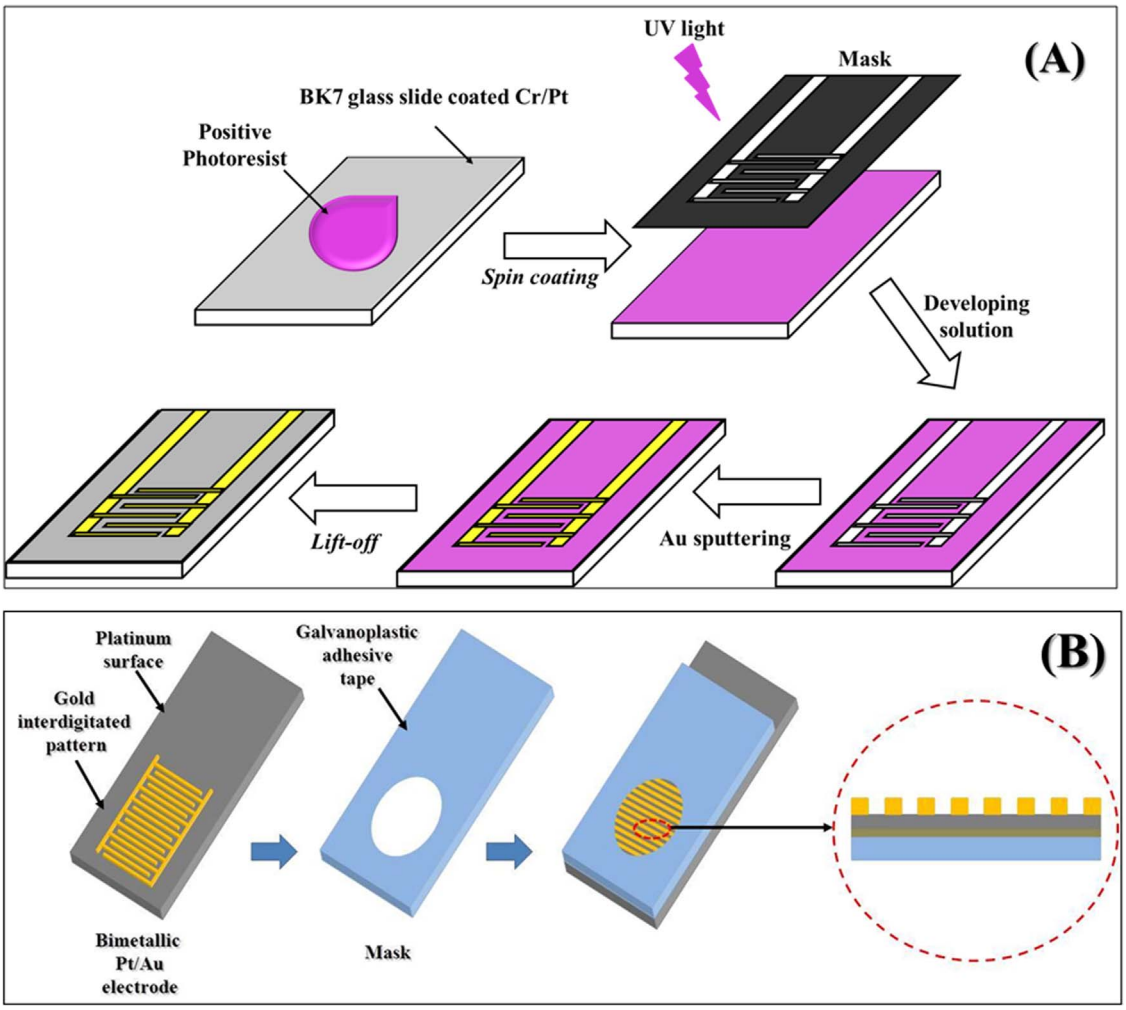

Fig. 1. – **(A)** schematic diagram of the experimental set-up. **(B)** schematic representation of Pt/Au bimetallic electrodes with a defined geometric area.

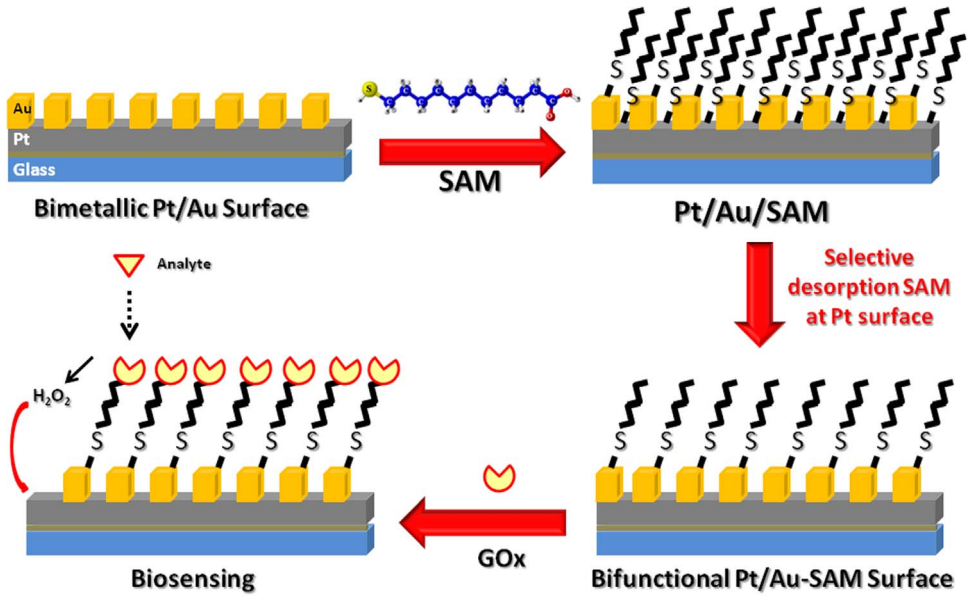

Fig. 2. – Schematic representation of Pt/Au bimetallic electrode coated with MUA-SAM on which GOx molecules are adsorbed. Also represented in the last cartoon (in clockwise direction) is the biosensing mechanism with H_2O_2 being generated from the interaction between GOx and the glucose analyte.

H_2O_2 will be formed from the enzymatic reaction in the areas with Pt only. In fact, even if some GOx molecules are adsorbed on the areas of bare Pt, they will be denatured and will not yield a H_2O_2 signal, which was confirmed in subsidiary experiments. In additional subsidiary control experiments, bare gold and platinum electrodes (geometric area 0.032 cm^2) were used.

Glucose oxidase was immobilized using the covalent bond method (Bankar et al., 2009; Cao et al., 2013b; Susanto et al., 2013) with EDC/NHS. The Pt/Au-SAM-GOx$_{selective\ desorption}$ bifunctional surface acquired a yellow color indicating that the amino groups from GOx molecules were bonded to carboxyl groups of the SAM. The biofilm remained stable on the device surface.

2.7. Analytical Procedure

The Pt/Au-SAM-GOx$_{selective\ desorption}$ bifunctional surface and control experiments using i) bare Pt, Au and Pt/Au; ii) Pt-GOx, Au-GOx and Pt/Au-GOx; iii) Pt/SAM-GOx, Au/SAM-GOx and Pt/Au/SAM-GOx (without selective desorption) electrodes were evaluated to detect glucose by CV. Analytical curves were then constructed by adding small volumes of concentrated standard solutions of glucose into the electrochemical cell containing 20 mL of 0.1 mol L^{-1} phosphate buffer solution (pH 7.0). The accuracy of the proposed method was verified from repeatability studies inter-day (n =5)) and intra-day (n =10).

Analyses of glucose in artificial saliva samples were carried out using triplicate samples of a modified form of Fusayama's artificial saliva,(Bagda and Tuzen, 2015; Fusayama et al., 1963) consisting of 0.081 g of $CaCl_2 0 \cdot 2H_2O$, 0.078 g $NaH_2PO_4 0 \cdot 2H_2O$, 0.043 g KCl, 0.04 g NaCl, 0.1 g urea, 1 mL of 0.05% of $Na_2S \cdot 9H_2O$ in 100 mL of distilled water. An aliquot of 5 µL of artificial saliva was added into the voltammetric cell containing 20 mL of phosphate buffer, pH 7.0, and homogenized with a magnetic stirrer. The cyclic voltammograms were recorded in the potential range from –0.2 to +0.6 V with a scan rate of 50 mV s^{-1}.

3. RESULTS AND DISCUSSION

3.1. Patterning Pt electrodes with nanostructured Au films

The deposition of Au patterns of three thicknesses on a Pt electrode was successful, as indicated in the AFM images of Fig. S1. The calculated values confirm that the average width and thickness of the Au patterns were obtained according to the design, with the three average thicknesses being close to the nominal values. The SEM images in Fig. S2 in the Supporting Information show that the Au films were almost defect-free.

Fig. 3(A) shows cyclic voltammograms (CV) for the Pt/Au bimetallic electrode, compared to those obtained of bare Pt and Au electrodes separately. The CV for Pt (a) features two redox pairs between –230 and +200 mV vs. Ag/AgCl, assigned to hydrogen (H_{ads}) adsorption and desorption processes on the Pt surface (Angerstein-Kozlowska et al., 1973; Santos and Tremiliosi, 2001). The anodic and cathodic peaks at 600–800 and 430 mV are due to oxidation (formation) and reduction of Pt oxides, respectively (Angerstein-Kozlowska et al., 1973; Santos and Tremiliosi, 2001). The CV in (**b**) is typical of Au in 0.1 mol L^{-1} H_2SO_4 solution (Angerstein-Kozlowska et al., 1986; Bruckenstein and Shay, 1985), with anodic and cathodic peaks at +1.15 V (E_{pa}) and +0.82 V (E_{pc}), assigned to oxidation and reduction of Au oxides(Angerstein-Kozlowska et al.,1986; Bruckenstein and Shay, 1985), respectively. For the Au-patterned Pt electrode (Pt/Au), curve (**c**) shows all the peaks observed for neat Au or Pt, thus confirming the formation of bimetallic nanostructures. The shift of 5 mV in the H_{ads} peaks is due to the increased Pt/Au film resistivity, which can be inferred by the smaller slope in the beginning of the Pt/Au voltammogram compared to that of pure Pt. It is worth mentioning that this increase in resistivity is not related to the charge-transfer resistance obtained in EIS. The peaks had reduced currents, since the presence of gold promotes a decrease in the Pt redox process. Note also that if potentials above 1.30 V are applied the coatings could be peeled off and the glass would be exposed (see Fig. S3 in the Supplementary Material).

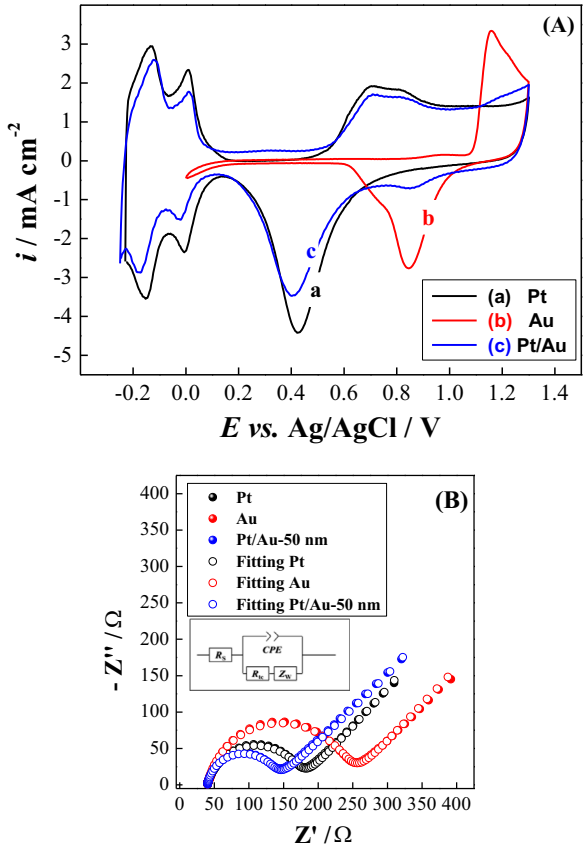

Fig. 3. – (A) Cyclic voltammograms in 0.1 mol L^{-1} H_2SO_4 solution for three electrodes: bare Pt (**a**), bare Au (**b**) and Au-patterned Pt electrode (Pt/Au) (**c**), where the Au film was 50 nm thick. Scan rate 1000 mV s^{-1}. **(B)** Complex plane impedance spectra for bare Au **(a),** Pt **(b)** and Pt/Au (Au 50 nm thick) **(c)** electrodes. The measurements were performed in 0.1 mol L^{-1} KCl solution containing 5.0×10^{-3} mol L^{-1} of the redox probe $[Fe(CN)_6]^{4-/3-}$. *Inset*: Equivalent circuit model used for analyzing the data.

The importance of patterning Pt with Au films became apparent in the increased electron transfer, compared to bare Pt and Au electrodes, as inferred from EIS measurements. Fig. 3 (B) shows the impedance spectra as complex plane plots (Nyquist diagrams) for the three types of electrode. The diagrams consisting of semicircles and diffusion straight lines were analyzed with a Randles modified equivalent circuit $[R_s(CPE[R_{ct}Z_W])]$, where R_s is the solution resistance, R_{ct} is the charge transfer resistance, Z_W is the Warburg impedance and CPE is a constant phase element. The apparent heterogeneous electron rate constant was determined using $k_{app} = RT/F^2 R_{ct} CA$, in which F is the Faraday constant (96,485.34 C mol^{-1}), C is the probe redox concentration in solution (5.0 mmol L^{-1}), R is the gas constant (8.3145 J K mol), T is the temperature (298 K), A is the geometric area (0.283 cm^2) and R_{ct} is the charge-transfer resistance obtained by fitting the data. k_{app} values calculated for bare Pt, bare Au and Pt/Au are listed in Table S1. R_{ct} is smaller for Pt/Au because of the synergy achieved in having Pt and Au sites for electron transfer (Chen et al., 2015). The increase of 37% in k_{app} for the Pt/Au electrode confirms the improvement in electron transfer when compared to Pt and Au bare surfaces, and this has important implications for the performance of electroanalytical devices, in addition to the bifunctional properties of this architecture.

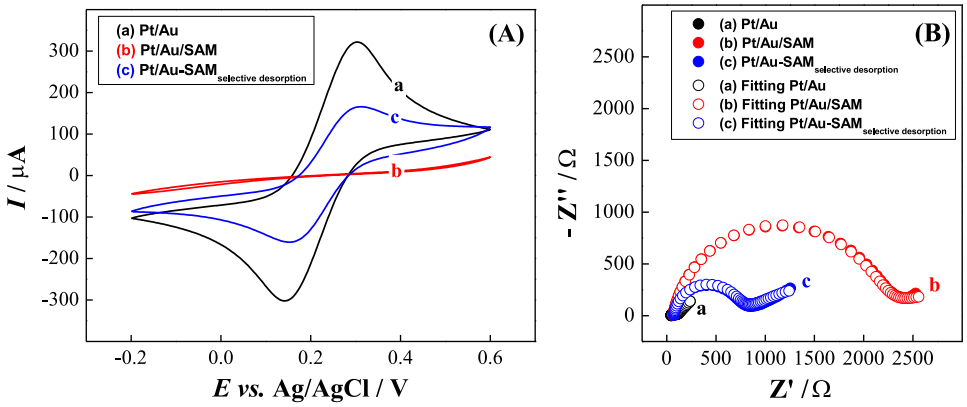

Fig. 4. – **(A)** Cyclic voltammograms obtained in 0.1 mol L^{-1} KCl solution containing 5.0 mmol L^{-1} $[Fe(CN)_6]^{-4/3-}$ at a scan rate 50 mV s^{-1}. **(B)** Nyquist diagram for **(a) Pt/Au**, (Au 50 nm thick). **(b) Pt/Au/SAM** and **(c) Pt/Au-SAM-GOx$_{selective\ desorption}$**, from impedance spectroscopy measurements.

3.2. *Exploiting Pt/Au bimetallic electrodes in glucose biosensors*

In order to take advantage of the enhanced electron transfer provided by the bimetallic nature of Pt/Au electrodes, we had to adsorb glucose oxidase selectively only on the Au patterns. This was performed by coating Pt/Au substrates with a self-assembled monolayer (SAM), which was selectively desorbed from the Pt surface via voltammetric cycling in a H_2SO_4 solution as described in Section 2.6. Fig. S4 in the Supporting Information brings the CV plots demonstrating that the blocking SAM layer can be removed from Pt, but not from Au surface, when cycling is performed up to 1.1 V vs. Ag/AgCl.

The result of this selective desorption of the SAM monolayer is seen in the CV and impedance spectra of Fig. 4(A), where the data are compared to the Pt/Au electrode fully coated with a SAM (Pt/Au/SAM) and to that one containing SAM only on the Au patterns (Pt/Au-SAM-GOx$_{selective\ desorption}$). The anodic and cathodic peaks at 0.303 and 0.152 V in Fig. 4(A) are assigned to electron transfer

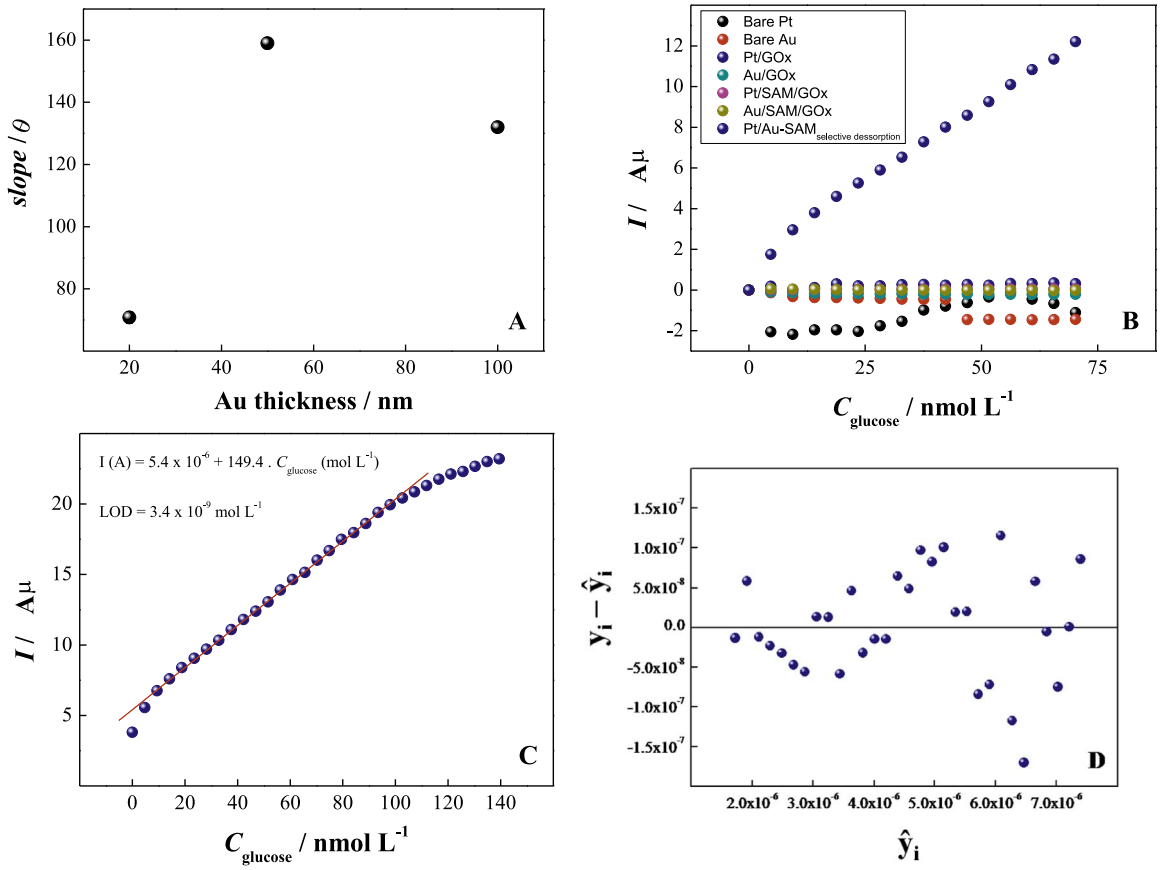

Fig. 5. – **(A)** – Slope of least-squares line (linear regression, $b = \sum[(x_i - x)(y_i - \bar{y})]/\sum(x_i - x)^2$) of the analytical curves obtained for glucose detection with (20, 50 and 100 nm) Au thickness of interdigitated fingers of the Pt/Au-SAM-GOx$_{selective\ desorption}$ bifunctional surface. Conditions: 0.1 M phosphate buffer solution, pH 7.0. **(B)** Analytical curves for glucose detection on different surfaces (control experiments) for the concentration range between 0 and 70 nmol L^{-1}. **(C)** Analytical curve for Pt/Au-SAM-GOx$_{selective\ desorption}$ bifunctional surface for the concentration range between 0 and 139.4 nmol L^{-1}. Conditions: 0.1 M phosphate buffer solution, pH 7.0. **(D)** – Residual plots in regression diagnosis. The coefficient of variation was of 1.7%.

between the bimetallic surface and the $[Fe(CN)_6]^{4-/3-}$ redox probe. They are clearly defined for the bare Pt/Au, but vanish when blocking takes place with the SAM (Pt/Au/SAM). Partial recovery of the peaks is seen for the Pt/Au-SAM-$GOx_{selective\ desorption}$ electrode owing to the exposed area of Pt surface after the selective desorption of the SAM. As expected, the blocking and selective SAM desorption affected the impedance spectra strongly, as indicated in Fig. 4(B). The Nyquist diagrams were fitted with a modified Randles circuit, whose parameters are given in Table S2. It is worth noting that the charge transfer resistance increased from 53 for Pt/Au to 1,873 Ω with SAM deposition (Pt/Au/SAM), and then decreased to 606 Ω after the selective removal of the SAM from Pt (Pt/Au-SAM-$GOx_{selective\ desorption}$). Based on these results, we estimate that 65% of the Pt/Au-SAM electrode area are uncoated, i.e. it is a Pt surface. This area corresponds to the geometric area that was not covered with gold electrodes, consistent with the values inferred from the micrographs.

The electrodes with selective adsorption of SAM, namely Pt/Au-SAM-$GOx_{selective\ desorption}$ bifunctional surface, were used for covalent bonding of glucose oxidase to detect glucose, where the enzyme was only bonded on the Au patterns coated with SAM. Subsidiary experiments were made to determine that a thickness of 50 nm for the Au patterning provided the best performance, in which we calculated the slope of the least-squares line of the analytical curves for glucose detection with interdigitated fingers of the Pt/Au-SAM-$GOx_{selective\ desorption}$ bifunctional surface. Fig. 5A shows that the slope (correlating with sensitivity) increased when the Au thickness changed from 20 to 50 nm because of an increased number of active sites with a larger amount of GOx adsorbed. However, if the Au thickness was increased further to 100 nm, the even larger amount of immobilized GOx may restrain peroxide diffusion to the Pt surface, thus decreasing the sensitivity. We made a systematic, comparative analysis of cyclic voltammograms in detecting glucose with bare surfaces (Pt, Au and Pt/Au), coated with GOx (Pt/GOx, Au/GOx and Pt/Au/GOx) and SAM-GOx (Au/SAM/GOx and Pt/SAM/GOx) and Pt/Au-SAM-$GOx_{selective\ desorption}$ bifunctional surface. Representative cyclic voltammograms are shown in Fig. S5 (in the Supporting Information), where it is clear that the reduction current (0 V vs. Ag/AgCl) recorded with the Pt/Au-SAM-$GOx_{selective\ desorption}$ bifunctional surface is the highest (Fig. S5H). The mechanism of detection is described as follows (Nakabayashi et al., 2006). First, glucose oxidase converts glucose into gluconolactone, which spontaneously hydrolyzes to gluconic acid, with H_2O_2 being also formed. The latter can be monitored by the electrocatalytic oxidation, i.e $\cdot H_2O_2 \rightarrow 2OH^-$ (Crespilho et al., 2006) and/or electrocatalytic reduction of the oxygen reduction about 0.0 V vs. Ag/AgCl (Chen et al., 2012a; Kung et al., 2014; Liu et al., 2010; Yang et al., 2011). Fig. 5B shows the calibration plots for the bare and modified surfaces in the glucose concentration range between 0 and 70×10^{-9} mol L^{-1}. The Pt/Au-SAM-$GOx_{selective\ desorption}$ bifunctional surface exhibited the most sensitive response with the largest slope of 159 A mol^{-1} L, and was the only surface with good linear relationship between peak current and glucose concentration. The cathodic peak current (the analytical signals were extracted from Fig. S6) increased almost linearly with the glucose concentration between 0 and 139.4×10^{-9} mol L^{-1}, as shown in Fig. 5C. Taking the linear part between 4.7 and 102.7 nmol L^{-1}, a calibration curve was represented by I (μA) = 5.4 (μA) + 149.4 (μA nM^{-1}) $C_{glucose}$ (nmol L^{-1}) with a linear correlation (r) of 0.999. The residual plots in Fig. 5D shows a satisfactory distribution of residuals except for $y25$ and $y26$, which might be two outliers, thus demonstrating the correctness of the linear regression.

The selective desorption on the Pt/Au-SAM-$GOx_{selective\ desorption}$ bifunctional surface facilitates electron transfer between peroxide and the electrode surface, owing to synergy between Au and Pt (Cesarino et al., 2015). The peak current is also higher for the Pt/Au-SAM-$GOx_{selective\ desorption}$ bifunctional surface because it has a platinum (SAM-free) surface and thus larger electroactive surface area than all the other surfaces. The platinum-free area serves for the transfer of electrons between the peroxide molecule and the electrode surface, and appears to dominate the electrochemical behavior of Pt/Au-SAM-$GOx_{selective\ desorption}$ bifunctional surface in detecting glucose. This is consistent with the R_{CT} value inferred from EIS measurements, thus confirming that the formation of the hybrid surface does not seem to induce extra structural disorder and/or defects onto the surface.

The detection limit (LOD) was calculated according to the statistical method described by Miller (Miller, 1991; Vicentini et al., 2016), defined as LOD $= a + 3\ S_{y/x}$, where a is the intercept and $S_{y/x}$ is the standard deviation of y-residuals of least-squares line (linear regression). The sensitivity was calculated from the slope of the least-squares line (linear regression), $b = \sum[(x_i - x)(y_i - \bar{y})]/\sum(x_i - x)^2$ (Raymundo-Pereira et al., 2016a; Raymundo-Pereira et al., 2016c; Vicentini et al., 2016). The limit of detection (LOD) for glucose was 3.4×10^{-9} mol L^{-1}. The reproducibility and repeatability of the Pt/Au-SAM-$GOx_{selective\ desorption}$ bifunctional surface were tested using the CV technique. The measurements were performed ten times in the presence of a redox probe with the same surface and with ten different surfaces prepared at room temperature under the same conditions. There was no significant loss of electrocatalytic activity with relative standard deviations (RSD) of 1.3% and 1.7%, respectively. Table S3 and S4 show that the Pt/Au-SAM-$GOx_{selective\ desorption}$ bifunctional surface exhibits higher performance than other sensors reported in the literature (Zhang et al., 2010), (Luo et al., 2010), (Zheng et al., 2010), (Liu et al., 2010), (Wang et al., 2011), (Crespilho et al., 2006), (Ngeontae et al., 2009), (Du et al., 2007), (Wu et al., 2007), (Kang et al., 2007), (Chen et al., 2012a) and (Cao et al., 2013a).

Another figure of merit to assess biosensing performance (Raymundo-Pereira et al., 2016b) is the rate of enzyme-substrate intermediate dissociation without conversion of the substrate into the product with the apparent Michaelis–Menten kinetic constant (K_M^{app})(Johnson and Goody, 2011; Vicentini et al., 2013). The probability of product formation per binding is inversely proportional to K_M^{app}, which may be obtained by linear regression using the Lineweaver–Burk equation (Kamin and Wilson, 1980; Lineweaver and Burk 1934; Shu and Wilson 1976): $I_{ss}^{-1} = I_{max}^{-1} + K_M^{app}\ I_{max}^{-1}\ [glucose]^{-1}$, where I_{ss} is the steady-state current measured for the enzymatic product and I_{max} is the maximum current under conditions of substrate (glucose) saturation. Since K_M^{app} was determined under steady-state conditions when $[S] \gg K_M$, then the equation $v_0 = V_{max}\ [S]/K_M + [S]$ reduces to $v_0 \approx V_{max}$. The equation of the Lineweaver–Burk plots for the Pt/Au-SAM-$GOx_{selective\ desorption}$ bifunctional surface was $I_{ss}^{-1} = 3.7 \times 10^5 + 1.6\ C_{glucose}^{-1}$ (correlation coefficient of 0.997). K_M^{app} was obtained by multiplying the slope ($1/I_{ss}$ vs $1/[glucose]$) by I_{max}. I_{max} and K_M^{app} in this study were 2.1×10^{-6} A and 3.2×10^{-6} mol L^{-1}, respectively.

3.3. Real Sample Analysis and Interference of Coexisting Substances

Artificial saliva samples were used to validate the proposed Pt/Au-SAM-$GOx_{selective\ desorption}$ bifunctional surface for glucose detection. Since artificial saliva samples dissolved in PBS solution did not present electroanalytical signals, glucose was spiked to the solution and a recovery of 95–105% of the added analyte was obtained. Potential interfering compounds in saliva, such as ascorbic acid, uric acid and dopamine, were also investigated with a fixed glucose concentration of 1.4×10^{-7} mol L^{-1}. Fig. S7 shows voltammograms for glucose and including interferents: 1.4, 2.8, 4.2×10^{-6} mol L^{-1} of ascorbic acid; 5.5, 1.1, 1.7×10^{-6} mol L^{-1} of

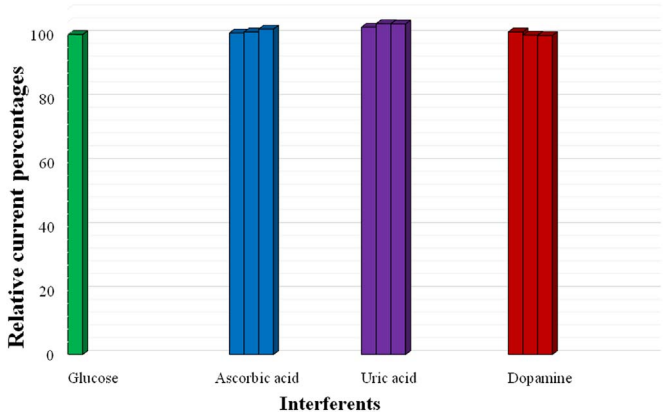

Fig. 6. – Effect of biomarkers ascorbic acid, uric acid and dopamine on the voltammetric responses for 1.4×10^{-7} mol L^{-1} glucose in artificial saliva samples with the Pt/Au-SAM-$GOx_{selective\ desorption}$ bifunctional surface. Conditions: 0.1 M phosphate buffer solution, pH 7.0. The coefficient of variation was 1.7%.

uric acid and 0.5, 1.0, 1.6×10^{-6} mol L^{-1} of dopamine. No additional analytical signals were observed for these interfering compounds within the ranges studied, which suggest the specificity of our system for glucose detection. Indeed, Fig. 6 shows the relative percentages in change in current for glucose detection in artificial saliva samples, where the values are essentially the same for glucose and interferent-containing glucose solutions. Interference was estimated as 0.5, 0.8 and 1.7; 2.3, 3.4 and 3.3; 0.8, −0.15 and −0.29% for ascorbic acid, uric acid and dopamine, respectively. This indicates that there are no co-adsorption processes on the Pt/Au-SAM-$GOx_{selective\ desorption}$ bifunctional surface.

4. CONCLUSIONS

The methods chosen to pattern the Pt surface with interdigitated Au fingers were proven suitable, as indicated by SEM and AFM images where both film thickness and distance between fingers could be controlled. Using a selective adsorption of SAMs on the Au fingers, we produced a biosensor with GOx immobilized only on Au, whose final architecture is Pt/Au-SAM-$GOx_{selective\ desorption}$ bifunctional surface. This modified electrode was termed bifunctional because it allowed to simultaneously immobilize the biomolecule (GOx) on gold to catalyze glucose, and detect hydrogen peroxide on Pt sites. Synergy was achieved with the bimetallic surface, which was manifested in an apparent Michaelis-Menten rate constant of 3.2×10^{-6} mol L^{-1}, considerably lower than commonly reported in the literature. The high catalytic activity of the Pt/Au-SAM-$GOx_{selective\ desorption}$ bifunctional surface led to a detection limit in the nanomolar range for glucose, and could also be used to determine glucose in artificial saliva samples. Significantly, the procedures adopted for producing the bimetallic, bifunctional surfaces are entirely generic and may be exploited in other bioelectronic devices.

Acknowledgments

The authors are thankful to CNPq and FAPESP (2012/17689–9, 2012/15543–7 and 2013/14262–7) for the financial support, and to FAPESP for the scholarships (2012/17689–9 and 2012/15543–7) to Paulo Augusto Raymundo-Pereira and Flávio M. Shimizu, respectively. Dr. Marcio de Paula is specifically acknowledged for the SEM micrographs.

Appendix A. Supplementary material

Supplementary data associated with this article can be found in the online version at http://dx.doi.org/10.1016/j.bios.2016.06.053.

References

Aliev, F.G., Correa-Duarte, M.A., Mamedov, A., Ostrander, J.W., Giersig, M., Liz-Marzan, L.M., Kotov, N.A., 1999. Layer-by-layer assembly of core-shell magnetite nanoparticles: Effect of silica coating on interparticle interactions and magnetic properties. Adv. Mater. 11 (12), 1006–1010.
Angerstein-Kozlowska, H., Conway, B.E., Sharp, W.B.A., 1973. Real Condition of Electrochemically Oxidized Platinum Surfaces: Part I. Resolution of Component Processes. J. Electroanal. Chem. 43 (1), 9–36.
Angerstein-Kozlowska, H., Conway, B.E., Hamelin, A., Stoicoviciu, L., 1986. Elementary Steps of Electrochemical Oxidation of Single-Crystal Planes of Au-1. Chemical Basis of Processes Involving Geometry of Anions and the Electrode Surfaces. Electrochim. Acta 31 (8), 1051–1061.
Bagda, E., Tuzen, M., 2015. Determination of zirconium in water, dental materials and artificial saliva after surfactant assisted dispersive ionic liquid based microextraction. Rsc Adv. 5 (130), 107872–107879.
Bankar, S.B., Bule, M.V., Singhal, R.S., Ananthanarayan, L., 2009. Glucose oxidase - An overview. Biotechnol. Adv. 27 (4), 489–501.
Bruckenstein, S., Shay, M., 1985. An Insitu Weighing Study of the Mechanism for the Formation of the Adsorbed Oxygen Monolayer at a Gold Electrode. J. Electroanal. Chem. 188 (1–2), 131–136.
Cao, S.R., Zhang, L., Chai, Y.Q., Yuan, R., 2013a. Electrochemistry of cholesterol biosensor based on a novel Pt-Pd bimetallic nanoparticle decorated graphene catalyst. Talanta 109, 167–172.
Cao, S.S., Fang, L., Zhao, Z.Y., Ge, Y., Piletsky, S., Turner, A.P.F., 2013b. Hierachically Structured Hollow Silica Spheres for High Efficiency Immobilization of Enzymes. Adv. Funct. Mater. 23 (17), 2162–2167.
Carrette, L., Friedrich, K.A., Stimming, U., 2000. Fuel cells: Principles, types, fuels, and applications. Chemphyschem 1 (4), 162–193.
Cavalcanti, I.T., Guedes, M.I.F., Sotomayor, M.D.P.T., Yamanaka, H., Dutra, R.F., 2012. A label-free immunosensor based on recordable compact disk chip for early diagnostic of the dengue virus infection. Biochem. ENG J. 67, 225–230.
Cesarino, I., Cincotto, F.H., Machado, S.A.S., 2015. A synergistic combination of reduced graphene oxide and *anti*mony nanoparticles for estriol hormone detection. Sens. Actuat B-Chem. 210, 453–459.
Chen, K.J., Lee, C.F., Rick, J., Wang, S.H., Liu, C.C., Hwang, B.J., 2012a. Fabrication and application of amperometric glucose biosensor based on a novel PtPd bimetallic nanoparticle decorated multi-walled carbon nanotube catalyst. Biosens. Bioelectron. 33 (1), 75–81.
Chen, K.J., Pillai, K.C., Rick, J., Pan, C.J., Wang, S.H., Liu, C.C., Hwang, B.J., 2012b. Bimetallic PtM (M = Pd, Ir) nanoparticle decorated multi-walled carbon nanotube enzyme-free, mediator-less amperometric sensor for H2O2. Biosens. Bioelectron. 33 (1), 120–127.
Chen, T.T., Ge, C.W., Zhang, Y.H., Zhao, Q., Hao, F.R., Bao, N., 2015. Bimetallic platinum-bismuth nanoparticles prepared with silsesquioxane for enhanced electrooxidation of formic acid. Int. J. Hydrog. Energ. 40 (13), 4548–4557.
Cho, S.J., Kauzlarich, S.M., Olamit, J., Liu, K., Grandjean, F., Rebbouh, L., Long, G.J., 2004. Characterization and magnetic properties of core/shell structured Fe/Au nanoparticles. J. Appl. Phys. 95 (11), 6804–6806.
Coelho, D., Machado, S.A.S., 2014. New contribution in the study of phase formation in mixed alkanethiol self-assembled monolayers: a powerful tool for transducers design. Electrochim. Acta 142, 191–201.
Crespilho, F.N., Ghica, M.E., Florescu, M., Nart, F.C., Oliveira, O.N., Brett, C.M.A., 2006. A strategy for enzyme immobilization on layer-by-layer dendrimer-gold nanoparticle electrocatalytic membrane incorporating redox mediator. Electrochem Commun. 8 (10), 1665–1670.
Du, D., Chen, S., Cai, J., Zhang, A., 2007. Immobilization of acetylcholinesterase on gold nanoparticles embedded in sol-gel film for amperometric detection of organophosphorous insecticide. Biosens. Bioelectron. 23 (1), 130–134.
Evans, S.A.G., Elliott, J.M., Andrews, L.M., Bartlett, P.N., Doyle, P.J., Denuault, G., 2002. Detection of hydrogen peroxide at mesoporous platinum microelectrodes. Anal. Chem. 74 (6), 1322–1326.
Ferapontova, E.E., Grigorenko, V.G., Egorov, A.M., Borchers, T., Ruzgas, T., Gorton, L., 2001. Mediatorless biosensor for H2O2 based on recombinant forms of horseradish peroxidase directly adsorbed on polycrystalline gold. Biosens. Bioelectron. 16 (3), 147–157.
Freeman, R.G., Hommer, M.B., Grabar, K.C., Jackson, M.A., Natan, M.J., 1996. Ag-clad Au nanoparticles: Novel aggregation, optical, and surface-enhanced Raman scattering properties. J. Phys. Chem. -Us 100 (2), 718–724.
Fusayama, T., Nomoto, S., Katayori, T., 1963. Corrosion of Gold and Amalgam Placed in Contact with Each Other. J. Dent. Res. 42 (5), 1183–&..
Hrapovic, S., Liu, Y.L., Male, K.B., Luong, J.H.T., 2004. Electrochemical biosensing platforms using platinum nanoparticles and carbon nanotubes. Anal. Chem. 76 (4), 1083–1088.
Jia, H., Gao, P., Ma, H., Wu, D., Du, B., Wei, Q., 2015. Preparation of Au-Pt nanostructures by combining top-down with bottom-up strategies and application in

label-free electrochemical immunosensor for detection of NMP22. Bioelectrochemistry 101, 22–27.
Johnson, K.A., Goody, R.S., 2011. The Original Michaelis Constant: Translation of the 1913 Michaelis-Menten Paper. Biochem. -Us 50 (39), 8264–8269.
Kamin, R.A., Wilson, G.S., 1980. Rotating-Ring-Disk Enzyme Electrode for Biocatalysis Kinetic-Studies and Characterization of the Immobilized Enzyme Layer. Anal. Chem. 52 (8), 1198–1205.
Kang, X.H., Mai, Z.B., Zou, X.Y., Cai, P.X., Mo, J.Y., 2007. A novel glucose biosensor based on immobilization of glucose oxidase in chitosan on a glassy carbon electrode modified with gold-platinum alloy nanoparticles/multiwall carbon nanotubes. Anal. Biochem. 369 (1), 71–79.
Karthikeyan, B., Murugavelu, M., 2012. Nano Bimetallic Ag/Pt System as Efficient opto and Electrochemical Sensing Platform towards Adenine. Sens. Actuat B-Chem. 163 (1), 216–223.
Kung, C.C., Lin, P.Y., Buse, F.J., Xue, Y.H., Yu, X., Dai, L.M., Liu, C.C., 2014. Preparation and characterization of three dimensional graphene foam supported platinum-ruthenium bimetallic nanocatalysts for hydrogen peroxide based electrochemical biosensors. Biosens. Bioelectron. 52, 1–7.
Lineweaver, H., Burk, D., 1934. The determination of enzyme dissociation constants. J. Am. Chem. Soc. 56, 658–666.
Link, S., Wang, Z.L., El-Sayed, M.A., 1999. Alloy formation of gold-silver nanoparticles and the dependence of the plasmon absorption on their composition. J. Phys. Chem. B 103 (18), 3529–3533.
Liu, X.Y., Zeng, X.D., Mai, N.N., Liu, Y., Kong, B., Li, Y.H., Wei, W.Z., Luo, S.L., 2010. Amperometric glucose biosensor with remarkable acid stability based on glucose oxidase entrapped in colloidal gold-modified carbon ionic liquid electrode. Biosens. Bioelectron. 25 (12), 2675–2679.
Luo, L.Q., Li, Q.X., Xu, Y.H., Ding, Y.P., Wang, X., Deng, D.M., Xu, Y.J., 2010. Amperometric glucose biosensor based on NiFe2O4 nanoparticles and chitosan. Sens. Actuat B-Chem. 145 (1), 293–298.
Manso, J., Mena, M.L., Yanez-Sedeno, P., Pingarron, J.M., 2008. Bienzyme amperometric biosensor using gold nanoparticle-modified electrodes for the determination of inulin in foods. Anal. Biochem. 375 (2), 345–353.
Miller, J.N., 1991. Basic Statistical-Methods for Analytical-Chemistry.2. Calibration and Regression Methods - a Review. Analyst 116 (1), 3–14.
Mott, D., Luo, J., Njoki, P.N., Lin, Y., Wang, L.Y., Zhong, C.J., 2007. Synergistic activity of gold-platinum alloy nanoparticle catalysts. Catal. Today 122 (3–4), 378–385.
Nakabayashi, Y., Hirosaki, Y., Yamauchi, O., 2006. Dipolar ruthenium(II) ammine complexes as electron transfer mediators of amperometric glucose sensors. Bioelectrochemistry 69 (2), 216–222.
Ngeontae, W., Janrungroatsakul, W., Maneewattanapinyo, P., Ekgasit, S., Aeungmaitrepirom, W., Tuntulani, T., 2009. Novel potentiometric approach in glucose biosensor using silver nanoparticles as redox marker. Sens. Actuat B-Chem. 137 (1), 320–326.
Park, S., Wieckowski, A., Weaver, M.J., 2003. Electrochemical infrared characterization of CO domains on ruthenium-decorated platinum nanoparticles. J. Am. Chem. Soc. 125 (8), 2282–2290.
Pumera, M., Sanchez, S., Ichinose, I., Tang, J., 2007. Electrochemical nanobiosensors. Sens. Actuat B-Chem. 123 (2), 1195–1205.
Qian, L., Yang, X.R., 2006. Polyamidoamine dendrimers-assisted electrodeposition of gold-platinum bimetallic nanoflowers. J. Phys. Chem. B 110 (33), 16672–16678.
Rashid, M., Jun, T.S., Jung, Y., Kim, Y.S., 2015. Bimetallic core-shell Ag@Pt nanoparticle-decorated MWNT electrodes for amperometric H-2. Sens. Direct Methanol Fuel cells Sens. Actuat B-Chem. 208, 7–13.
Raymundo-Pereira, P.A., Lima, A.R.F., Machado, S.A.S., 2016a. A nanostructured label-free platform based on an ultrathin film for ultrasensitive detection of a secosteroid hormone. Rsc Adv. 6 (41), 34458–34467.
Raymundo-Pereira, P.A., Mascarenhas, A.C.V., Teixeira, M.F.S., 2016b. Evaluation of the Oxo-bridged Dinuclear Ruthenium Ammine Complex as Redox Mediator in an Electrochemical Biosensor. Electroanal 28 (3), 562–569.
Raymundo-Pereira, P.A., Campos, A.M., Prado, T.M., Furini, L.N., Boas, N.V., Calegaro, M.L., Machado, S.A.S., 2016c. Synergy between Printex nano-carbons and silver nanoparticles for sensitive estimation of antioxidant activity. Anal. Chim. Acta 926 (5), 88–98.
Ricci, F., Palleschi, G., 2005. Sensor and biosensor preparation, optimisation and applications of Prussian Blue modified electrodes. Biosens. Bioelectron. 21 (3), 389–407.
Sanedrin, R.G., Georganopoulou, D.G., Park, S., Mirkin, C.A., 2005. Seed-mediated growth of bimetallic prisms. Adv. Mater. 17 (8), 1027-+.
Santos, V.P., Tremiliosi, G., 2001. The correlation between the atomic surface structure and the reversible adsorption-desorption of hydrogen on single crystal Pt (111), Pt (100) and Pt (110) electrodes. Quim. Nova 24 (6), 856–863.
Shu, F.R., Wilson, G.S., 1976. Rotating-Ring-Disk Enzyme Electrode for Surface Catalysis Studies. Anal. Chem. 48 (12), 1679–1686.
Susanto, H., Samsudin, A.M., Rokhati, N., Widiasa, I.N., 2013. Immobilization of glucose oxidase on chitosan-based porous composite membranes and their potential use in biosensors. Enzym. Microb. Tech. 52 (6–7), 386–392.
Tkac, J., Davis, J.J., 2008. An optimised electrode pre-treatment for SAM formation on polycrystalline gold. J. Electroanal. Chem. 621 (1), 117–120.
Trindade, T., O'Brien, P., Pickett, N.L., 2001. Nanocrystalline semiconductors: Synthesis, properties, and perspectives. Chem. Mater. 13 (11), 3843–3858.
Uliana, C.V., Tognolli, J.O., Yamanaka, H., 2011. Application of Factorial Design Experiments to the Development of a Disposable Amperometric DNA Biosensor. Electroanal. 23 (11), 2607–2615.
Upadhyay, S., Rao, G.R., Sharma, M.K., Bhattacharya, B.K., Rao, V.K., Vijayaraghavan, R., 2009. Immobilization of acetylcholineesterase-choline oxidase on a gold-platinum bimetallic nanoparticles modified glassy carbon electrode for the sensitive detection of organophosphate pesticides, carbamates and nerve agents. Biosens. Bioelectron. 25 (4), 832–838.
Vicentini, F.C., Janegitz, B.C., Brett, C.M.A., Fatibello-Filho, O., 2013. Tyrosinase biosensor based on a glassy carbon electrode modified with multi-walled carbon nanotubes and 1-butyl-3-methylimidazolium chloride within a dihexadecylphosphate film. Sens. Actuat B-Chem. 188, 1101–1108.
Vicentini, F.C., Raymundo-Pereira, P.A., Janegitz, B.C., Machado, S.A.S., Fatibello, O., 2016. Nanostructured carbon black for simultaneous sensing in biological fluids. Sens. Actuat B-Chem. 227, 610–618.
Wang, J., 2005. Nanomaterial-based electrochemical biosensors. Analyst 130 (4), 421–426.
Wang, W.Q., Ying, S.H., Zhang, Z.H., Huang, S.S., 2011. Novel glucose biosensor based on a glassy carbon electrode modified with hollow gold nanoparticles and glucose oxidase. Microchim Acta 173 (1–2), 143–148.
Wojtysiak, S., Solla-Gullon, J., Dluzewski, P., Kudelski, A., 2014. Synthesis of core-shell silver-platinum nanoparticles, improving shell integrity. Colloid Surf. A 441, 178–183.
Wu, B.Y., Hou, S.H., Yin, F., Zhao, Z.X., Wang, Y.Y., Wang, X.S., Chen, Q., 2007. Amperometric glucose biosensor based on multilayer films via layer-by-layer self-assembly of multi-wall carbon nanotubes, gold nanoparticles and glucose oxidase on the Pt electrode. Biosens. Bioelectron. 22 (12), 2854–2860.
Wu, Z.Y., Chen, L.G., Shen, G.L., Yu, R.Q., 2006. Platinum nanoparticle-modified carbon fiber ultramicroelectrodes for mediator-free biosensing. Sens. Actuat B-Chem. 119 (1), 295–301.
Yang, L., Zhao, H., Fan, S.M., Deng, S.S., Lv, Q., Lin, J., Li, C.P., 2014. Label-free electrochemical immunosensor based on gold-silicon carbide nanocomposites for sensitive detection of human chorionic gonadotrophin. Biosens. Bioelectron. 57, 199–206.
Yang, M.H., Yang, Y.H., Liu, Y.L., Shen, G.L., Yu, R.Q., 2006. Platinum nanoparticles-doped sol-gel/carbon nanotubes composite electrochemical sensors and biosensors. Biosens. Bioelectron. 21 (7), 1125–1131.
Yang, Z.J., Ren, Y.Y., Zhang, Y.C., Li, J., Li, H.B., Hu, X.C.H.X.Y., Xu, Q., 2011. Nanoflake-like SnS2 matrix for glucose biosensing based on direct electrochemistry of glucose oxidase. Biosens. Bioelectron. 26 (11), 4337–4341.
Yoo, S.H., Park, S., 2007. Platinum-coated, nanoporous gold nanorod arrays: Synthesis and characterization. Adv. Mater. 19 (12), 1612-+.
Yu, S.J., Wei, Q., Du, B., Wu, D., Li, H., Yan, L.G., Ma, H.M., Zhang, Y., 2013. Label-free immunosensor for the detection of kanamycin using Ag@Fe3O4 nanoparticles and thionine mixed graphene sheet. Biosens. Bioelectron. 48, 224–229.
Zhang, Y.F., Guo, G.P., Zhao, F.Q., Mo, Z.R., Xiao, F., Zeng, B.Z., 2010. A Novel Glucose Biosensor Based on Glucose Oxidase Immobilized on AuPt Nanoparticle - Carbon Nanotube - Ionic Liquid Hybrid Coated Electrode. Electroanal 22 (2), 223–228.
Zheng, L.Z., Li, J.H., Xu, J.P., Xiong, L.Y., Zheng, D., Liu, Q., Liu, W., Li, Y.D., Yang, S.M., Xia, J., 2010. Improvement of amperometric glucose biosensor by the immobilization of FcCD inclusive complex and carbon nanotube. Analyst 135 (6), 1339–1344.